International Journal on Interactive Design and Manufacturing (IJIDeM)
https://doi.org/10.1007/s12008-023-01702-0

ORIGINAL ARTICLE

Optimization of ultrasonic assisted friction stir welding (UAFSW) of electrical grade AA 6101T-64 and Cu

Sharad Nirgude[1] · **Shyamkumar Kalpande**[2]

Received: 31 May 2023 / Accepted: 9 December 2023

Abstract
Ultrasonic assisted friction stir welding (UAFSW) of electrical grade aluminum alloy 6101 (T-64) and pure Cu plates was performed with Box–Behnken design matrix and optimized by response surface methodology. Tool rotational speed, machine table traverse speed, tool pin offset, and tool tilt angle are taken into account as experimental parameters since they play a key role in the formation of sound weld joints. The correlation between UAFSW input process parameters and output response variables (ultimate tensile strength σ_s and electrical resistivity ρ) is studied in this research work by developing the mathematical models. In order to maximize or minimize the responses, the process is optimized. The interface effects of the UAFSW input process parameters on the output responses variables are interpreted using the response plots generated using the mathematical models. Analysis of variance (ANOVA) is used to verify the established models. As per the ANOVA table, the tool rotational speed and tool pin offset were the significant input process parameters for σ_s of the weld joint. On the other hand, it was observed that all the parameters were significant for ρ. Good agreement was seen between the experiment results and the predicted models of the research. The microhardness evaluation showed the variations in the distribution of microhardness in top zone, middle zone, and bottom zone of the weld joint cross section. Peak microhardness distribution was observed in the top zone of the weld joint cross section followed by middle zone and bottom zone.

Keywords UAFSW · Box–Behnken design matrix · RSM · UTS · Electrical resistivity · Microhardness distribution

List of symbols

N	Tool rotational speed
S	Traverse speed
O	Tool pin offset
A	Tool tilt angle
TSD	Tool shoulder diameter
P_P	Pin profile
P_d	Pin diameter
P_l	Pin length
kHz	Frequency
μm	Vibration amplitude
σ_s	Ultimate tensile strength
ρ	Electrical resistivity
ϕ	Diameter
SZ	Stir zone
HAZ	Heat affected zone
TMAZ	Thermomechanically affected zone

✉ Sharad Nirgude
snirgude299@gmail.com

Shyamkumar Kalpande
shyamkalpande@gmail.com

[1] Department of Mechanical Engineering, MET's IOE Bhujbal Knowledge City, Nashik, India

[2] Department of Mechanical Engineering, Guru Gobind Singh COE and RC, Nashik, India

1 Introduction

The dissimilar Al-Cu joint is widely used in lightweight structures as a cost-effective, weight-reduction, and environmental protection measure in aerospace, nuclear, electronics and electrical industries [1–3]. Aluminum and copper both exhibit excellent mechanical and electrical properties [4]. However, the physical and chemical properties of both materials are different [5, 6]. Fusion welding is not able to produce sound weld joints of dissimilar Al and Cu because of physical and chemical differences between them. Fusion welding of such materials results in high residual stress, weld cracking,

Published online: 16 January 2024

and the production of hard and brittle intermetallic compounds (IMCs) [2]. A green non-fusion solid state welding technique called friction stir welding (FSW) is used above the recrystallization temperature of the material; used for welding of similar as well as dissimilar materials like Al-Al Al-Mg, Al-Ti, Al-Steel, and Al-Cu [7–9]. A rotating tool with special profile pin and shoulder profile is inserted into the adjacent line of the workpiece plates and advances in the longitudinal direction. Heat is generated when a tool makes frictional contact with a workpiece, which causes the material to deform plastically and accelerates material flow [10]. The quality of FSW joints is still limited even though the method is efficient [2]. The growth of hard, brittle IMCs causes weak bonding between the dissimilar materials, which results in poor weld joint strength [11]. Mechanical properties, heat conduction, and electrical resistance are all affected by the formation of IMCs at the weld zone [12–14]. FSW also faces the difficulties like lower tool life when it is used for welding of high melting point materials. Frequently replacement of worn- out tool increases the production cost [1]. The closed cracks formation during FSW affects the fatigue life of the weld joint [15]. Several attempts have been made to supply supplementary sustaining energy to improve the weld joint's characteristics in order to address these issues with FSW. This includes introduction of induction coil and laser torch etc [1, 16]. The integration of ultrasonic vibrations with manufacturing processes has been found efficient to form sound weld joint formation [3]. Some defects like tunnel, cavity, and voids are formed during FSW because of wrong selection of input process parameters causes the improper stirring and insufficient heat input. To increase the effectiveness of the advanced manufacturing processes, ultrasonic vibrations have been used to help tooling in numerous manufacturing processes [1]. Utilising ultrasonic vibrations during turning and drilling operations reduced the resulting stresses and improved the state of the process [17]. In UAFSW of AZ91-C Mg alloy, with the help of ultrasonic vibrations the axial load was decreases by 6 to 17% which increases the tool life [18]. With the use of ultrasonic vibrations, the flow stress and stimulation energy of the material are reduced. It also stimulates the stability of plastic deformation in the area of weld zone observed during UAFSW of AA 6061—T6 and C11000 copper [2]. The strain energy and residual stress were found to be reduced by the ultrasonic vibration during FSW of AA 2219-T6 [19]. The ultrasonic vibrations gives fine grain structure and improves the UAFSW AZ91 joint tensile strength and microhardness [20]. The ultrasonic vibrations reduced the tool torque and traverse force. It also reduces the welding load with increase in the tool rotational speed seen in UAFSW of AA 2024-T3 [16]. In the welding process of Al and Mg alloy, it was seen that the ultrasonic vibration produces turbulence in the stirred zone of the weld joint and enhances the plastic deformation of the material. The axial force, tool torque are significantly reduces with the help of ultrasonic vibrations. It helps to lowers the defects formation in the SZ and it increases the strength of the weld joint [21]. The application of ultrasonic vibrations during the process smoothens the material flow, enhances the stirring in the SZ, and refines the sub grains, all of which lead to a superior weld quality of AA 6061-T6 [22]. It was seen that the ultrasonic vibrations assist in generation of higher heat in the SZ during welding process which accelerates the plastic deformation and material flow. Also it altered the microhardness level on the surface in friction stir processing (FSP) of AA 6061-T6 [23]. The mean grain size in the SZ of the weld joint is decreased by the use of ultrasonic vibration. It also provides the additional plasticizing effect on the welded metal which accelerates the stirring in the SZ observed in case of joining of AA 7075 alloy. Also, the positive impact of ultrasonic vibrations on both mechanical and tribological properties was observed while FSW of AA 6061 [3]. FSW of AA 6061 weld joint hardness and strength was increased with the increase in the magnitude of ultrasonic vibrations [24]. Due to enhanced stirring, the temperature is raised during FSW by ultrasonic vibration, which also reduces the welding force [25]. The tensile strength increased upto 25% and fatigue life was increased by 3 times with the use of ultrasonic vibrations during FSW of die cast alloy steel and AZ 80 Mg alloy [26]. The ultrasonic vibration significantly speeds up the welding process and enhances the FSW joint's surface quality [27]. The ultrasonic vibrations of 22 kHz frequency to the weld joint during FSW was seen very beneficial in uniform microhardness distribution in the weld joint of AA 2024 alloy and helps to attain higher tensile strength compare to FSW joint. It also provides better stirring with equiaxed recrystallized grains [28]. An introduction of ultrasonic vibrations during FSW of AZ 31 Mg alloy shown in reduction of axial forces and more uniform temperature distribution in the weld joint [29]. The ultrasonic vibrations are also helpful in FSW joints repairing to eliminate the defects like kissing bonds. It also seen to be improving the material flow and atom diffusion, and refines the grain structure in the SZ of the weld joint of 4 mmthick AZ31B alloy sheets [30]. The application of 20 kHz frequency of ultrasonic vibrations to the tool strengthens the plastic flow and increase the mixing intensity in the weld zone of Additional plasticising and blending of the material in the SZ improved the tensile strength of EN AW 5754 FSW joint [31]. Without affecting the mechanical characteristics of the weld joint, the application of ultrasonic vibrations greatly reduces the welding force. The traverse speed found prominent in the welding forces during friction stir lap welding of 3 mmthick of AA 6061–T6 sheets [10]. Pravin et. al. [32] optimized the shielded metal arc welding [SMAW] process with the assistance of vibratory system by using the Taguchi and analysis ANOVA. Enhancement in the hardness, tensile strength, and impact strength was seen with

the assistance of vibrating energy. At a constant tool rotational speed the ultrasonic vibrations enhances the material flow seen in FSW of AA 2024 [33]. The ultrasonic excitation decreases and homogeneously distributes the grains; observed in the laser beam welding of AA 6082 [34]. Ultrasonic vibration assistance in FSLW of AA 6061-T6 and 301 Lsteel alloy resulted in enhancement in the fluidity of the material. Also the reduction of IMC layer side from 10 to 6 μm and increase in tensile strength by 27% [11]. Vibrational application improves dynamic recrystallization, which results in a finer grain distribution. The strength, toughness, and hardness of the weld joint also improve [35]. The assistance of ultrasonic vibrations of 1.8 kW with 1200 rpm tool rotational speed and 150 mm/min traverse speed during FSW of AA 2219 showed the improvement in tensile strength of 10.5% [36]. Ultrasonic assisted aging in FSW of AA 2195 alloys showed the reduced grain size in the SZ of the weld joint [37]. The transmission of ultrasound in the FSW of Al and Mg influences the microstructure and corrosion behaviour. It limits the IMC phase formation which leads to increase the tensile strength [38]. Wazery et al. [39] optimized the UAFSW process parameters for highest weld joint efficiency. The optimum process parameters were; amplitude of ultrasonic vibrations 20 μm, tool rotational speed and traverse speed 800 rpm and 80 mm/min respectively. The tool rotational speed was seen the most important parameter for UAFSW. Husain Mehdi et. al. [40] optimized the FSW process parameters for joining of dissimilar AA 2014 and AA 6061 by RSM. The study revealed that the tool rotational speed and welding speed were significant parameters. The subgrain formation during FSW improved the strength of the weld joint. They also observed the refined grain structure in the SZ. Husain Mehdi et. al. [41] optimized the multi-pass FSP parameters for the fabrication of AA 6061 and Al_2O_3. Increase in the ultimate tensile strength and hardness was seen with increase in Al_2O_3 nanoparticles and number of FSP runs. Nait Salah et. al. [42] optimizes the FSW process parameters for dissimilar aluminum alloys AA 3003 and AA 6061 by RSM. The observations revealed that the tensile strength and hardness increased with increase in the tool rotational speed. Shaurya Bhatnagar et. al. [43] optimized the FSW process parameters for welding of dissimilar AA 7050 and AA 6061 using RSM. Their observations revealed that the tool rotational speed and welding speed are significant parameters which affect the strength of the weld joint. The extracted literature summary of various researchers related to process parameter is shown in Table 1.

A comparison of the characteristics of the FSW and UAFSW processes has been studied by numerous researchers. The research study was also carried on the mechanical and electrical properties of Al-Cu weld joint; whereas the optimization of process parameters is lacking in the previous research. The novelty & objectives of this research work are that it studies, optimizes, and analyses the effect of UAFSW process parameters on microhardness, tensile strength and electrical resistivity of the Al-Cu weld joint. The present configuration for research study is selected on the basis of the previous literature. The parameters and their levels which mostly influence the output responses of the UAFSW process were considered for experimentation.

2 Experimental procedure

The ultrasonic generator, transducer, and horn are the three components of the ultrasonic vibrator arrangement as shown in Fig. 1. Numerous trials have been carried out in order to choose the input parameter range. Four significant input parameters, three levels, and a Box–Behnken design matrix of RSM were selected for designing the experiment. Box–Behnken design is still considered to be more proficient and most powerful that other design, so considered for this study. It is used to generate higher order response surfaces using fewer required runs than a normal factorial technique. Box–Behnken designs are experimental designs for response surfcace methodology where each factor or independent variable is placed at one of three equally spaced values ususlly coaded as − 1,0, + 1.

Box–Behnken design matrix suggested 27 experimental runs using the significant number of influencing input parameters. The lower intermediate and higher limits of the input parameters were coded as − 1,0, + 1, and respectively in design matrix. In the present research study, FSW experiments were conducted on 4 mmthick Al and Cu sheets. The size of the each plate was 150 × 75 × 4 mm. To remove the thin oxidised coating from the plate surfaces, grit paper was used. Goose neck clamps provide secure holding and precise placement of the welding plates within the fixture. Tool details are as: Material—H13 (tool steel), P_P—tapered cylindrical, TSD—20 mm, P_d—(smaller ϕ: 5 mm, larger ϕ: 6 mm), taper angle: 10°49′15″, and P_l -3.7). Ultrasonic vibrations details are as: Frequency − 20 kHz and amplitude − 25 μm. The tool offset was et al. side. Cu material was placed at the advancing side whereas Al was placed at the retreating side. The actual experimental setup is shown in Fig. 2. The tool was plunged by 0.1 mm with 20 s dwell time. The UTS specimens were cut by WEDM in accordance with ASTM—E8 standard. Additionally, the wire cut EDM machine (WEDM) was used to cut the test specimens for electrical resistivity and microhardness. The microhardness test was performed with 100 g load for 15 s. Using a Vickers microhardness tester, the distribution of microhardness in the different weld joint zones is evaluated with the application of a load of 100 g for 15 s time duration. The specimen prepared for the tensile test in accordance with ASTM E8

Table 1 Literature summary of various researchers related to process parameter

Sr. no	Welded joints	Welding parameters					Tool parameters					ReferENCES
		N (rpm)	S (mm/min)	O (mm)	A (°)	μm	Tool mate-rial	TSD (mm)	P_d (mm)	P_l (mm)	P_P	
1	AA 2219	800	200–400	–	2.5	25	–	14	6	4.75	Conical	[19]
2	AA 2224	400–800	120–240	–	–	40	–	15	5.6	5.7	Conical	[16]
3	AA 6061	1200	50	–	–	25	H13	10	-	2.9	Conical	[21]
4	AA 6061	1200	160	–	–	26	–	6	4	2.2	Conical	[24]
5	AA 6061	500–1000	64–142	0	–	5	H13	15	3.5	–	Conical	[25]
6	AA 7N01	1200	80–240	–	–	10	–	16	8	5.8	Conical	[27]
7	AA 6082/Cu	1000	200	1.9–2.5	3	–	H13	16	5	2.9	Cylindrical	[44]
8	AA 2195	600	300	–	–	25	–	–	–	–	–	[37]
9	Al/Mg	–	–	–	–	35	–	16	–	3.1	Cylindrical threaded	[38]
10	AA 1050/Cu	600–1400	50–125	1–2	1.5	–	HSS	18	–	–	Cylindrical	[45]
11	AA 1100/Cu	1002	198	–	3	–	H13	10	3	1.7	Cylindrical	[8]
12	AA 1350/Cu	1000	80	2	2	–	HSS	16	5.2	–	Cylindrical threaded	[9]
13	AA 5082/Cu	1000	100	0	2	–	–	12	5.3	–	Conical	[12]
14	Pure Al/Cu	800	50	–	–	–	–	12	2.8	–	–	[13]
15	AA 5083/Cu	710	69	2	2	–	Cr. steel	18	6	5.9	Cylindrical threaded	[46]
16	AA 5083/Cu	750	160	–	2	–	H13	14	3	–	Cylindrical	[44]
17	Pure Al/Cu	600	50	–	–	–	H13	12	2.9	2.6	Cylindrical	[47]
18	AA 8011/Cu	550–950	100	0.5–1.5	1	–	HSS	20	6	2.6	Cylindrical	[14]
19	AA 6061/Cu	750	150	1.5	2.5	–	HSS	18	8	–	Conical	[48]
20	AA 6061/Cu	900	20–150	2	–	–	H13	11	5	3.8	Threaded	[49]
21	AA 1060/Cu	600	50	–	–	–	H13	20	8	4	Cylindrical	[50]

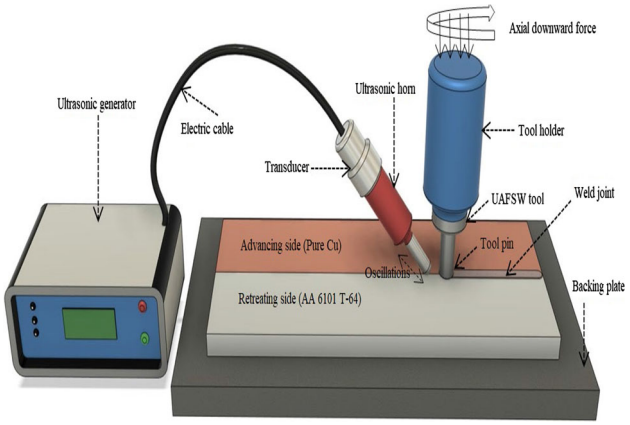

Fig. 1 Schematic of UAFSW process set up

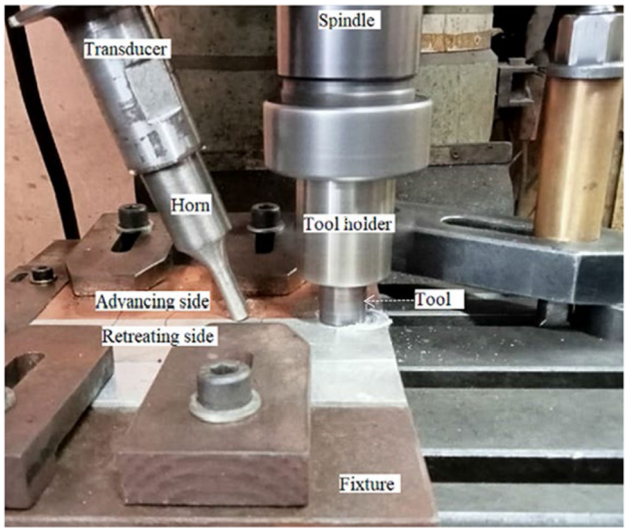

Fig. 2 Actual experimental set up

Fig. 3 ASTM E8 sample for tensile test [27, 51, 52]

and the sample for the electrical resistivity and microhardness tests are shown in Figs. 3 and 4 respectively. Table 2 shows the UAFSW input process parameters and their levels for experimentation. The Box–Behnken design matrix and experimental results are shown in Table 3.

3 Mathematical model development

The UAFSW input process parameters and the output response variables were mathematically associated by the

Fig. 4 Specimen for microhardness and electrical resistivity test [53]

RSM as follows [55–57]:

$$\text{UTS, } \sigma_s = \text{f (N, S, O, A)} \tag{1}$$

$$\text{Electrical resistivity, } \rho = \text{f (N, S, O, A)} \tag{2}$$

The second order polynomial regression equation for representing the response surface is expressed as follows:

$$Y = a_0 + \sum a_i x_i + \sum a_{ii} x_i^2 + \sum a_{ij} x_i y_i \tag{3}$$

Equation (3) can be be written as,

$$\begin{aligned} Y = {} & a_0 + a_1 N + a_2 S + a_3 O + a_4 A \\ & + a_{11} N^2 + a_{22} S^2 + a_{33} O^2 + a_{44} A^2 \\ & + a_{12} N\text{x}S + a_{13} N\text{x}O + a_{14} N\text{x}A \\ & + a_{23} S\text{x}O + a_{24} S\text{x}A + a_{34} O\text{x}A \end{aligned} \tag{4}$$

where a_0 is the mean value of output response variables whereas the coefficients a_1, a_2, a_3, and a_4 represents linear, quadratic and interaction coefficients respectively in the above equation. The coefficients a_{11}, a_{22}, a_{33}, and a_{44} are quadratic terms and the coefficients a_{12}, a_{13}, a_{14}, a_{23}, and b_{34} are interaction terms in the above equation. The evaluation and testing of the coefficients performed with a 95% confidence level. A mathematical model was created for the prediction of UTS as well as electrical resistivity of the weld joint [40, 55, 58].

$$\begin{aligned} \sigma_s = {} & -216.7 + 0.7672N + 0.711S + 23.4O + 10.46A \\ & - 0.000417N^2 - 0.00659S^2 - 14.48O^2 - 2.291A^2 \\ & + 0.000012N\text{x}S + 0.0085N\text{x}O - 0.00143N\text{x}A \\ & - 0.041S\text{x}O - 0.0232S\text{x}A + 1.14O\text{x}A \end{aligned} \tag{5}$$

Table 2 UAFSW input process parameters and their levels for experimentation [40, 42, 54]

Sr. no	Input process parameters	Notation of parameter	Levels		
			− 1	0	+ 1
1	Tool rotational speed (rpm)	N	700	900	1100
2	Traverse speed (mm/min)	S	30	50	70
3	Tool pin offset (mm)	O	0.6	0.9	1.2
4	Tool tilt angle (Degrees)	A	1	2	3

Table 3 Box–Behnken design matrix and experimental results [54]

Exp. run	Input Process Parameters				σ_s (MPa)	ρ (μΩm)
	N	S	O	A		
1	0	0	0	0	196.34	0.028
2	0	1	1	1	187.76	0.025
3	0	0	− 1	1	189.80	0.027
4	0	0	0	0	195.97	0.028
5	− 1	0	0	− 1	172.36	0.027
6	1	0	− 1	0	181.11	0.035
7	0	− 1	0	− 1	192.64	0.030
8	0	0	0	0	196.92	0.028
9	1	1	0	0	180.73	0.030
10	− 1	0	0	1	173.55	0.024
11	0	− 1	0	1	193.06	0.028
12	1	0	0	1	181.40	0.033
13	0	− 1	1	0	192.43	0.027
14	0	− 1	− 1	0	191.95	0.029
15	1	− 1	0	0	181.11	0.037
16	− 1	0	− 1	0	170.77	0.026
17	0	0	− 1	− 1	192.38	0.030
18	0	1	− 1	0	192.11	0.027
19	0	0	1	0	197.10	0.027
20	0	0	1	− 1	194.74	0.027
21	− 1	1	0	0	171.23	0.024
22	1	0	1	0	188.53	0.031
23	1	0	0	− 1	180.35	0.035
24	0	1	0	− 1	191.82	0.028
25	0	1	0	1	191.46	0.024
26	− 1	0	1	0	176.15	0.023
27	− 1	− 1	0	0	172.83	0.025

$$\begin{aligned}\rho = {} & 0.027956 + 0.004333N - 0.001465S \\ & - 0.001145O - 0.001158A + 0.001464N^2 \\ & - 0.000484S^2 - 0.000504O^2 + 0.000227A^2 \\ & - 0.001500N\text{x}S - 0.000250N\text{x}O + 0.000250N\text{x}A \\ & + 0.000104S\text{x}O - 0.000262S\text{x}A + 0.000777O\text{x}A \end{aligned} \quad (6)$$

4 UAFSW joint surface appearance at the validation test and the optimized weld joint

The weld joint surface appearance for the validation test is shown in Fig. 5. The dense flashes were seen as a result of the improved softening Fig. 5(a–e). Also the enhanced material

flow promotes faster material deformation during the process which results in oxidation observed on the Cu side. The same observations were seen during FSW of Al-Cu [8, 59]. Higher tool rotational speed was associated with smoother surface appearance. The same observations were noted by [59]. The significance of ultrasonic vibrations was seen at the optimized values input process parameters were as: tool rotational speed—930 rpm, traverse speed—47 mm/min, tool pin offset—1.10 mm, and tool tilt angle—2°; smoother surface appearance with slight shoulder marks were observed.

5 Microstructural analysis

Figure 6(a–o) shows optical microscopic images of different weld zones of validation test samples. Five experimental runs were performed for validation test. A stronger & sharper interfacial layer was observed at the retreating side (Al side) in the microscopic observations as shown in Fig. 6(a, d, g, j, m). The Cu material particles are obviously introduced in the retreating side which generates the interfacial layer [7]. The zigzag distribution of Al-Cu intermixing was seen as a result of intense distribution of Al-Cu in the SZ as shown in Fig. 6(h, k). The ultrasonic vibrations promote this distribution by improving the plastic flow of the material. The Al grains were significantly deformed and small equiaxed grains were also observed in this zone [60]. The heat generation and plastic deformation causes the refined grain structure in distinct HAZ and TMAZ of the weld joint. A refined grain structure was observed et al. side interface. The grains in the HAZ were seen larger and elongated in manner as compared to the grains in the TMAZ. The deformation width and area is improved with the assistance of ultrasonic vibrations. The improved plastic deformation and local thermal effect distributes the ultrafine grain structure [61].

On the other hand, at the advancing side (Cu side) different mixing behaviour was seen due to increase in heat supplied. This happens due higher coefficient of thermal expansion. Change in input parameters leads to different patterns of microstructure. A vortex like microstructure was seen in the SZ as shown in Fig. 6(b, h, n). A swirl like microstructure was observed in Fig. 6e. A zigzag structure with random distribution was seen in Fig. 6(k). Different recrystallized grain structure was seen at the Al-Cu interface of the advancing side. Equiaxed and finer grain structure was observed in the TMAZ whereas coarser and elongated grain structure was observed at the Cu side. It was also observed that the width of the TMAZ was varying with the change in the input process parameter as there was different heat supply at different experimental run. Figure 6(g, h, i) represents the microscopic images at higher tensile strength with refined grain structure at the interfacial layers and in the SZ. The ultrasonic vibration improves the material flow for intermixing of the material

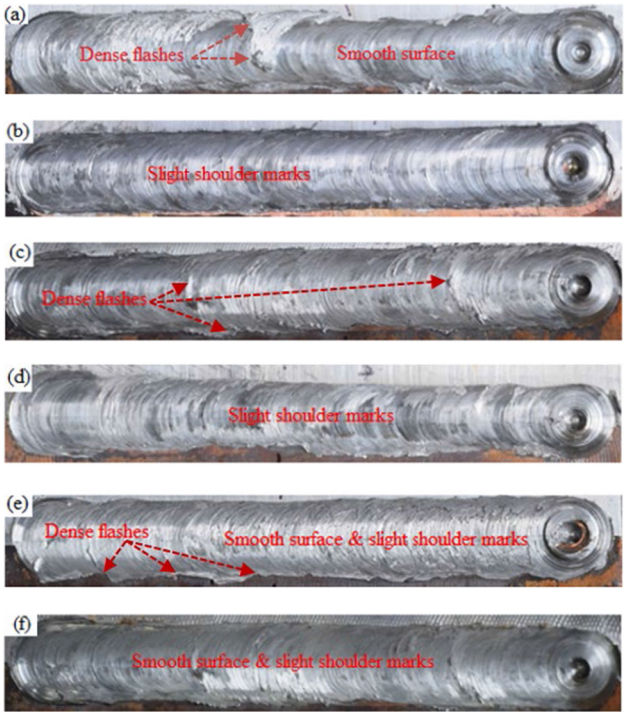

Fig. 5 Validation test joint surface appearance of (**a**–**e**). Surface appearance of the welded joint prepared at optimum UAFSW process parameters (**f**)

which results in higher tensile strength of the weld joint [7, 62].

6 Evolution of results

6.1 Significance of parameters on UTS

The effect of UAFSW parameters on the Al-Cu weld joint quality was examined using UTS testing. The interface effects of UAFSW input process parameters and UTS of weld joint are shown in Figs. 8 and 9. The UTS was improved and then reduced after reaching its extreme value as level of process parameters increases upto some level. The significance of N & S and O & A on σ_s is shown in Figs. 11 and 12 respectively. The scatter plots as shown Fig. 7(a, b, c, d) exhibits good agreement between UAFSW input process parameters and σs. Also it shows the linear relationship between N, S, O, A and σ_s.

6.1.1 Significance of rotational speed of the tool

The significance of rotational speed of the tool on UTS is shown in Fig. 10a. The UTS was comparatively low at 700 rpm tool rotational speed. It resulted from insufficient heating and mixing of the Cu elements in matrix of Al.

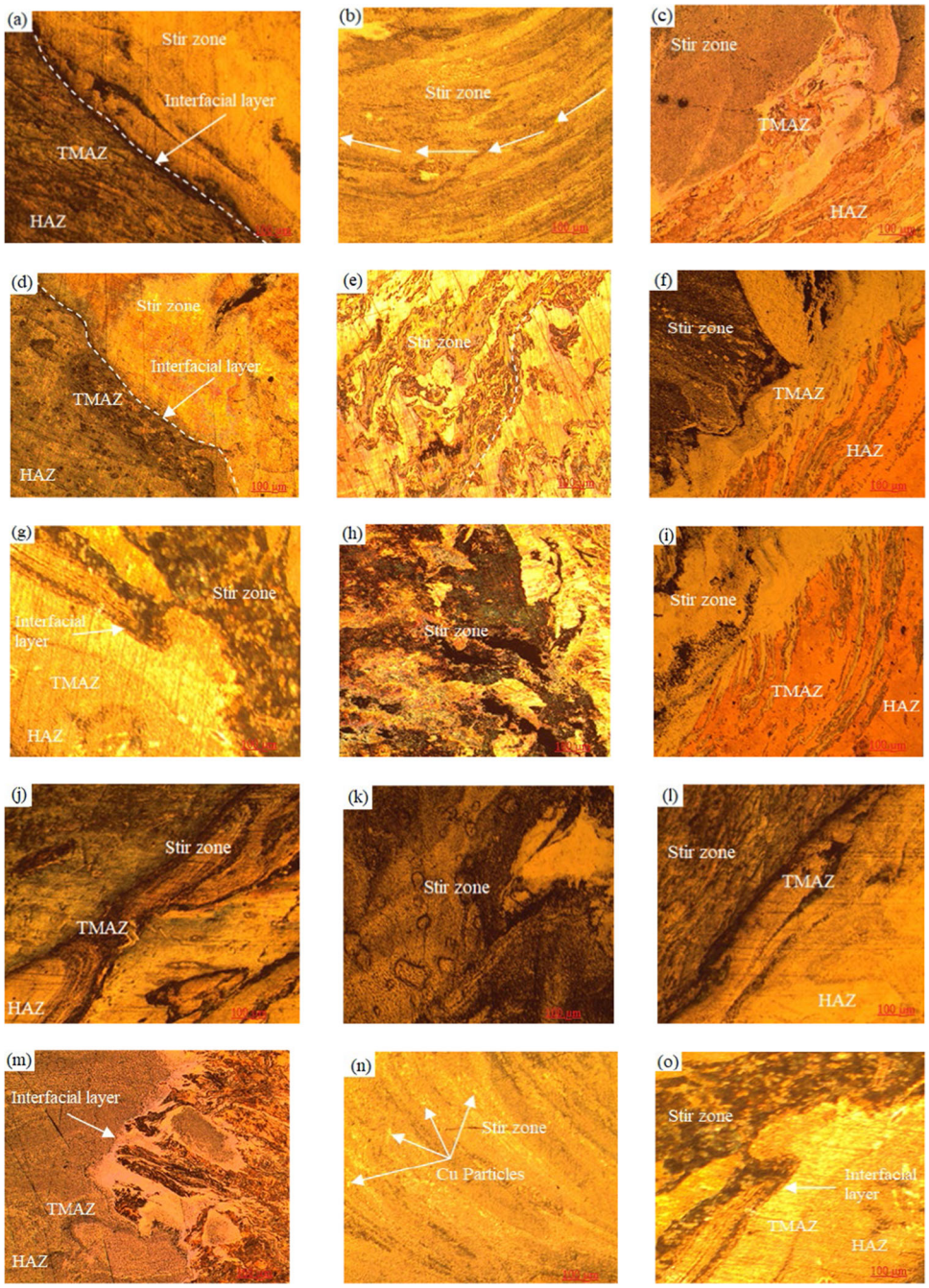

Fig. 6 Optical microscopic images of UAFSW validation test performed as per Table 5. (**a–c**) experimental run 1, (**d–f**) experimental run 2, (**g–i**) experimental run 3, (**j–l**) experimental run 4, and (**m–o**) experimental run 5

With increasing the rotational speed of the tool, the UTS of the weld joint progressively improved. At a 900 rpm speed, the Cu and Al matrix mixed adequately, leading to UTS of 197.10 MPa [12]. Higher tensile strength is attained as an effect of the ultrasonic vibrations reduces the size of the grains in the SZ, which causes the volumetric component of the grain borders to function as barriers against the movement of the grain dislocations [18]. UTS was decreasing as the rotational speed of the tool increased from 900 to 1100 rpm. The reason was more heat produced due to the shoulder face and base material plate coming into contact for an extensive period of time which encourages the thickening of IMCs in the SZ [63, 64]. High tool rotational speed resulted in a decrease in UTS and an increase in IMCs in the weld zone [12, 56, 65].

6.1.2 Significance of traverse speed

Lower UTS was observed at a 30 mm/min traverse speed due to too much heating. Also the flow stress difference between Al-Cu in the SZ because the turbulent material flow reduces strength, as shown in Fig. 10b. Maximum UTS was seen at

50 mm/min traverse speed; as the sufficient heat is supplied. The reduction in recrystallized fine grains size occurs as a result of the use of ultrasonic vibrations as it increases the grain boundary [18]. The turbulent flow is get normalised at 50 mm/min traverse speed. As the traverse speed rises to 70 mm/min, the heat input gets decreased. It decreases the speed of plasticization and inappropriate material mixing takes place in the weld joint. Hence, the weld joints failed at lower UTS.

6.1.3 Significance of tool pin offset

The significance of a tool pin offset towards Al side on the UTS of the weld joint is presented in Fig. 10c. Lower UTS was seen at the 0.6 mm tool pin offset due to weak bonding in the weld joint. As more Cu atoms are in the SZ, forming brittle IMC, which decreases the UTS [48]. The value of UTS was increased as tool pin offset was changed from 0.9 and 1.2 mm. The reason for that is lower IMCs formation due to fewer amounts of Cu atoms present in the SZ which reacts with the Al atoms. The UTS was increasing with increase in the tool pin offset value towards Al side upto 1.1 mm then decreased [12, 48, 65].

6.2 Measurement of electrical resistivity

Electrical resistivity of the weld joint was measured using the SIGMASCOPE apparatus. It was seen between 0.023 μΩm and 0.037 μΩm. A change in resistivity was seen during UAFSW because to differences in heat input, material mixing, and microstructure. The contour plots and surface plots in Figs. 13 and 14 shows the effect of process parameters on electrical resistivity of the weld joint. The direct effect plots in Fig. 15 show how the UAFSW parameters affect electrical resistivity of the weld joint. Figures 16 and 17 shows the interface effects of UAFSW input process parameters on the electrical resistivity. As the rotational speed of the tool increases, the electrical resistivity was raised. It was also seen that as traverse speed increased, the electrical resistivity decreased. The scatter plots as shown Fig. 18(a, b, c, d) exhibits good agreement between UAFSW input process parameters and ρ. Also it shows the linear relationship between N, S, O, A and ρ.

6.2.1 Significance of rotational speed of the tool

The significance of rotational speed of the tool on weld joint electrical resistivity is shown in Fig. 15a. A higher electrical resistivity was observed at the greater tool rotational speed of 1100 rpm. The increased heat input leads to thicken the IMCs at this temperature. Electrical resistivity increased as a result of IMCs. Due to the lack of heat supplied and the slightly increased thickness of the IMCs in the weld zone,

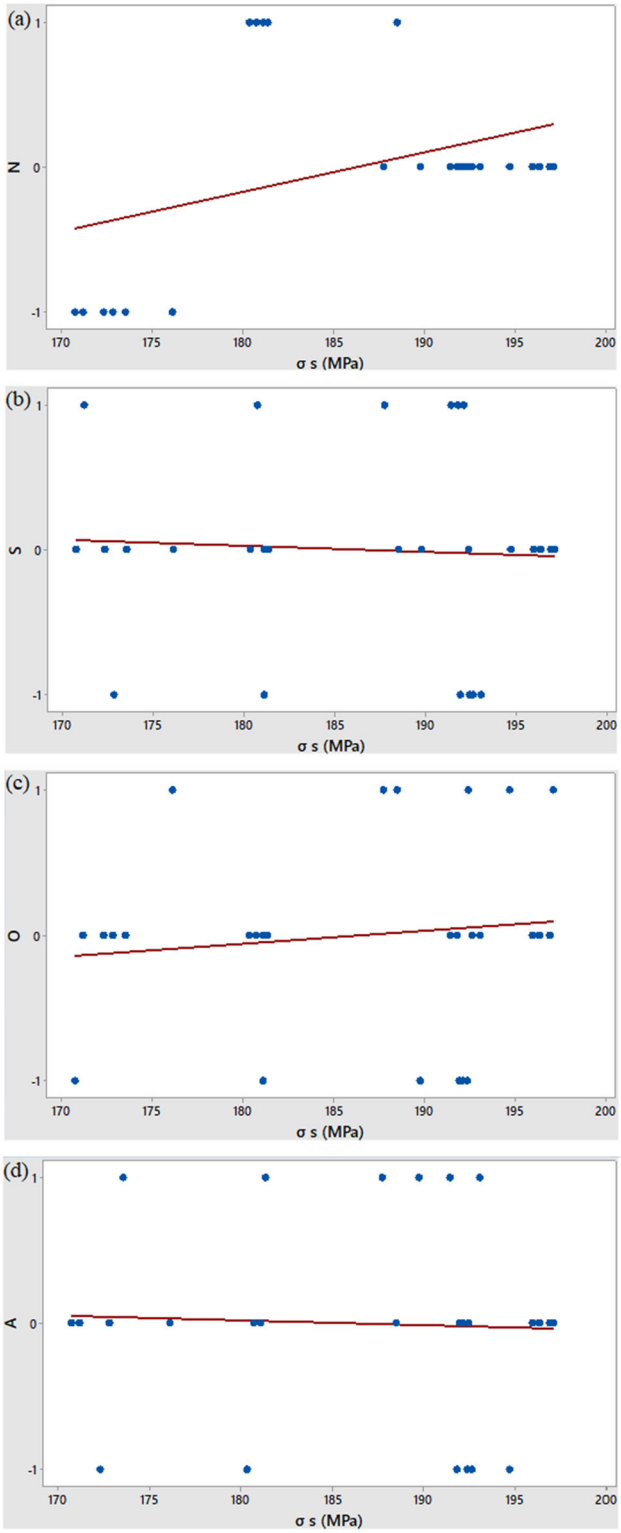

Fig. 7 Scatter plots of UAFSW input process parameters and σ_s. **a** N and σ_s. **b** S and σ_s. **c** O and σ_s. **d** A and σ_s

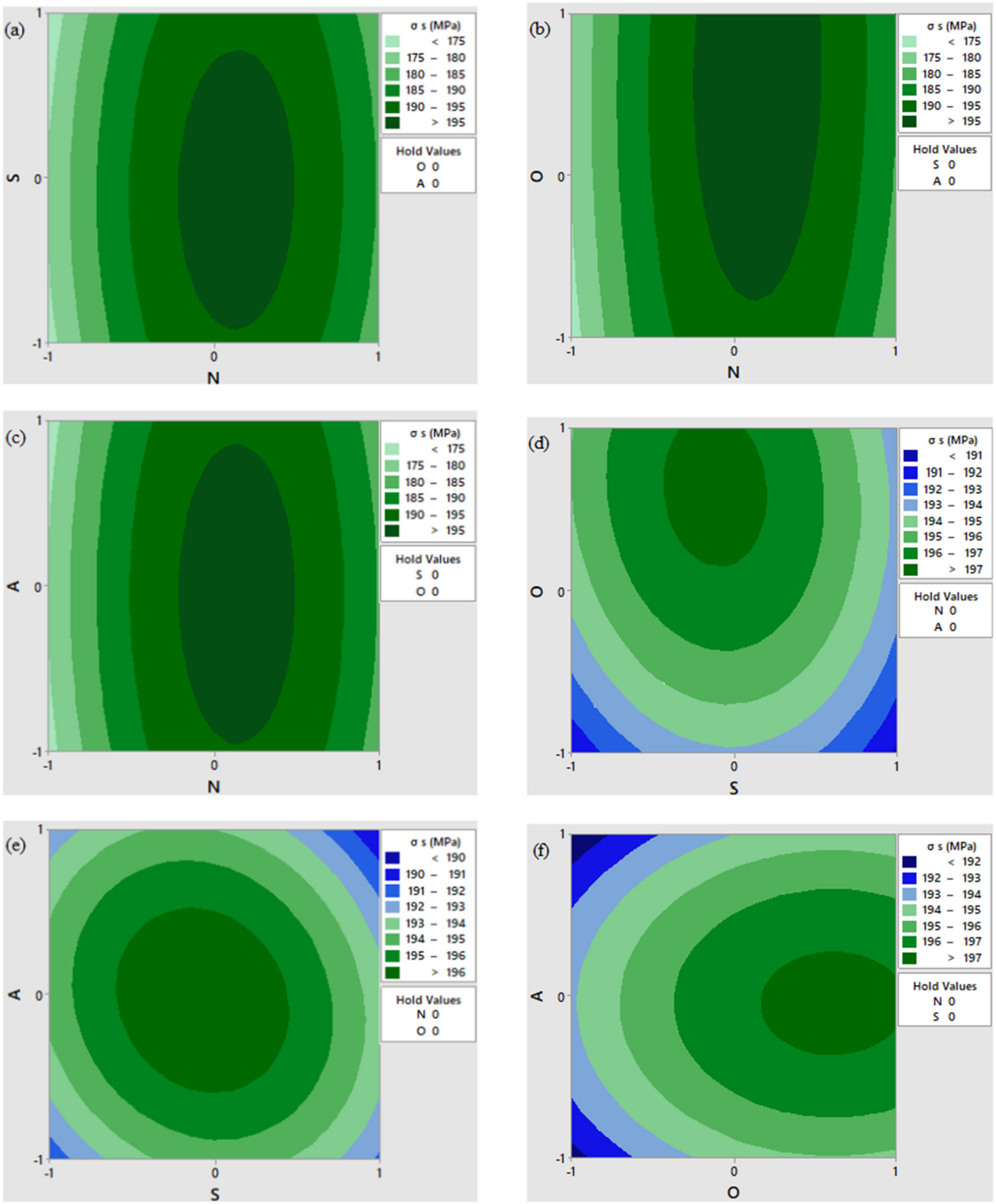

Fig. 8 Contour plots of UAFSW parameters and σ_s

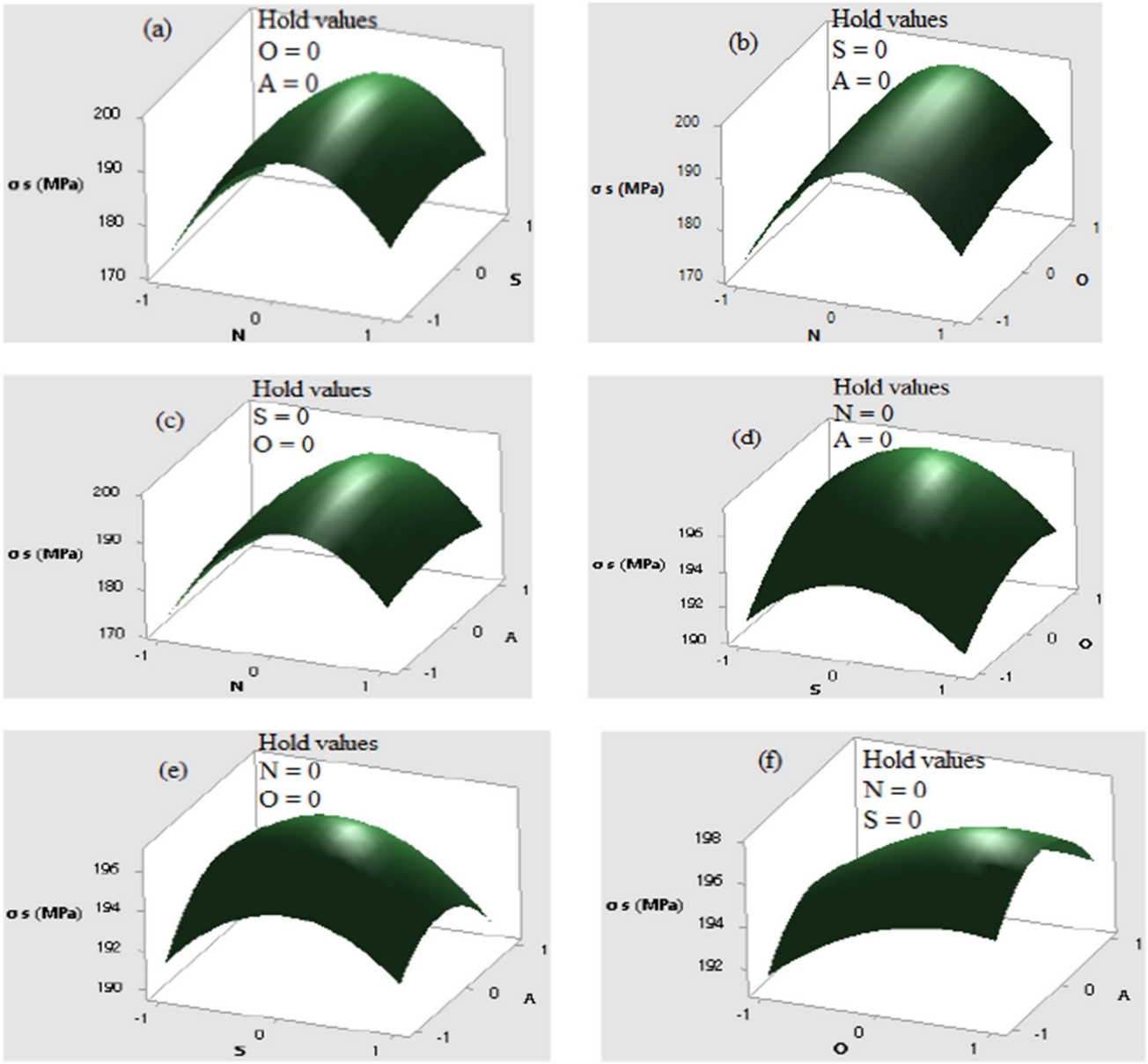

Fig. 9 Tensile strength response surface plots with UAFSW parameters

the lowermost electrical resistivity was found at the lowest tool rotational speed of 700 rpm [53, 63, 65].

6.2.2 Significance of traverse speed of welding process

Figure 15b presents the significance of traverse speed on electrical resistivity of the weld joint. Rotational speed of the tool and traverse speed was found significant parameters for the electrical resistivity of the welded joint as it impacts amount of heat is generated during the welding process. A greater electrical resistivity of 0.037 μΩm was observed at the 30 mm/min traverse speed of welding process. IMCs thickens IMCs thickened at this temperature [14, 44, 65]. In contrast, when heat input and IMC size similarly decrease, electrical resistivity at 70 mm/min traverse speed reduces by 0.023 μΩm.

6.2.3 Significance of tool pin offset

As more Cu particles contact with the Al matrix at the lesser tool pin offset in the direction of the Al side of the weld joint producing hard, thick, and brittle IMCs. Figure 15c shows the significance of tool pin offset towards Al side. A minimal number of Cu atoms blend with the matrix of Al as the tool pin offset moves more towards the Al side during welding, encouraging the production of lesser IMCs and a reduction in

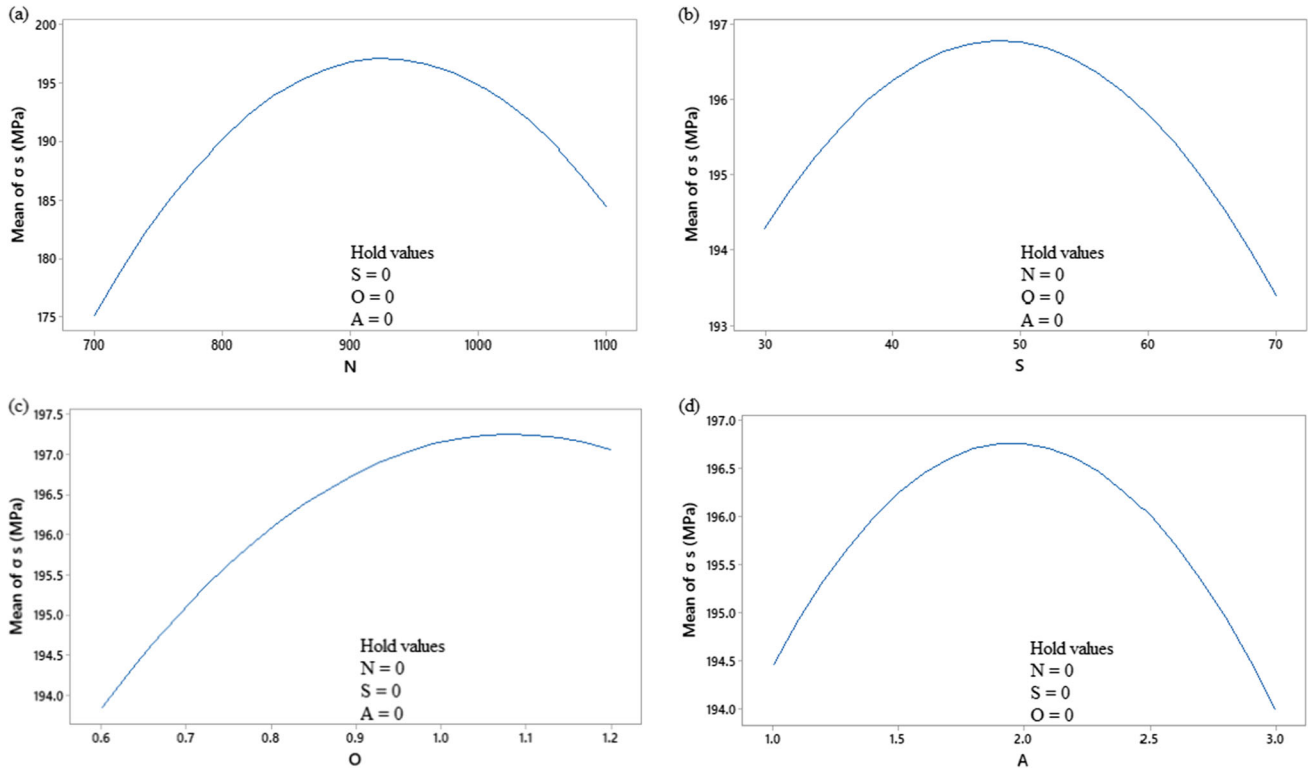

Fig. 10 Significance of UAFSW parameters on σ_s: **a** N, **b** S, **c** O, and **d** A

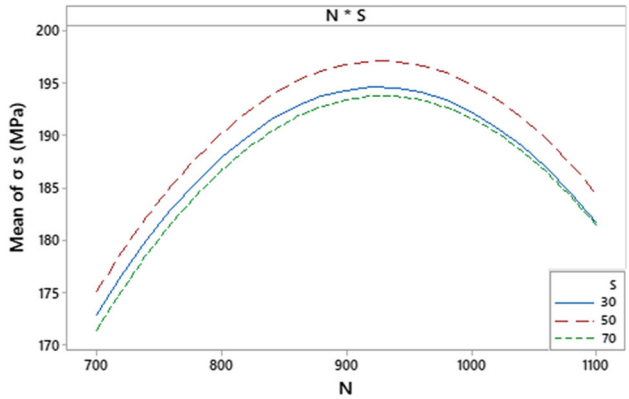

Fig. 11 Significance of N and S interrelating on σ_s

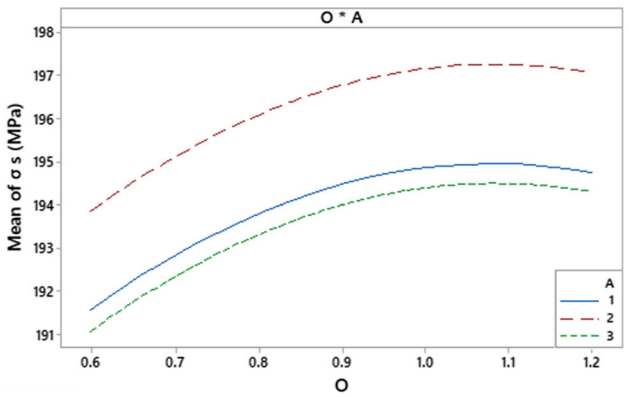

Fig. 12 Significance of O and A interrelating on σ_s

electrical resistivity [14, 53, 66]. The 0.6 mm tool pin offset in the direction of the Al side, maximum electrical resistivity of 0.037 μΩm was obtained. An electrical resistivity of 0.023 μΩm was found at 1.2 mm the tool pin offset on the Al side of the weld joint.

6.2.4 Significance of tilt angle of the tool

Figure 15d shows the significance of tilt angle of the tool on electrical resistivity of the weld joint. It was seen that as tool tilt angle was raised, the electrical resistivity of the weld joint decreased as heat input reduced. Because there are less intensity of IMCs formation because of the reduced heat supplied in the weld zone, there is a decrease in electrical resistivity [44, 63, 65, 67].

6.3 Competency of approved models for σ_s and ρ

The statistical findings of the established experimental correlations are displayed in Tables 4 and 8. The complete agreement between the predictable values and experimental values is demonstrated by R^2 value as 1. The statistical results

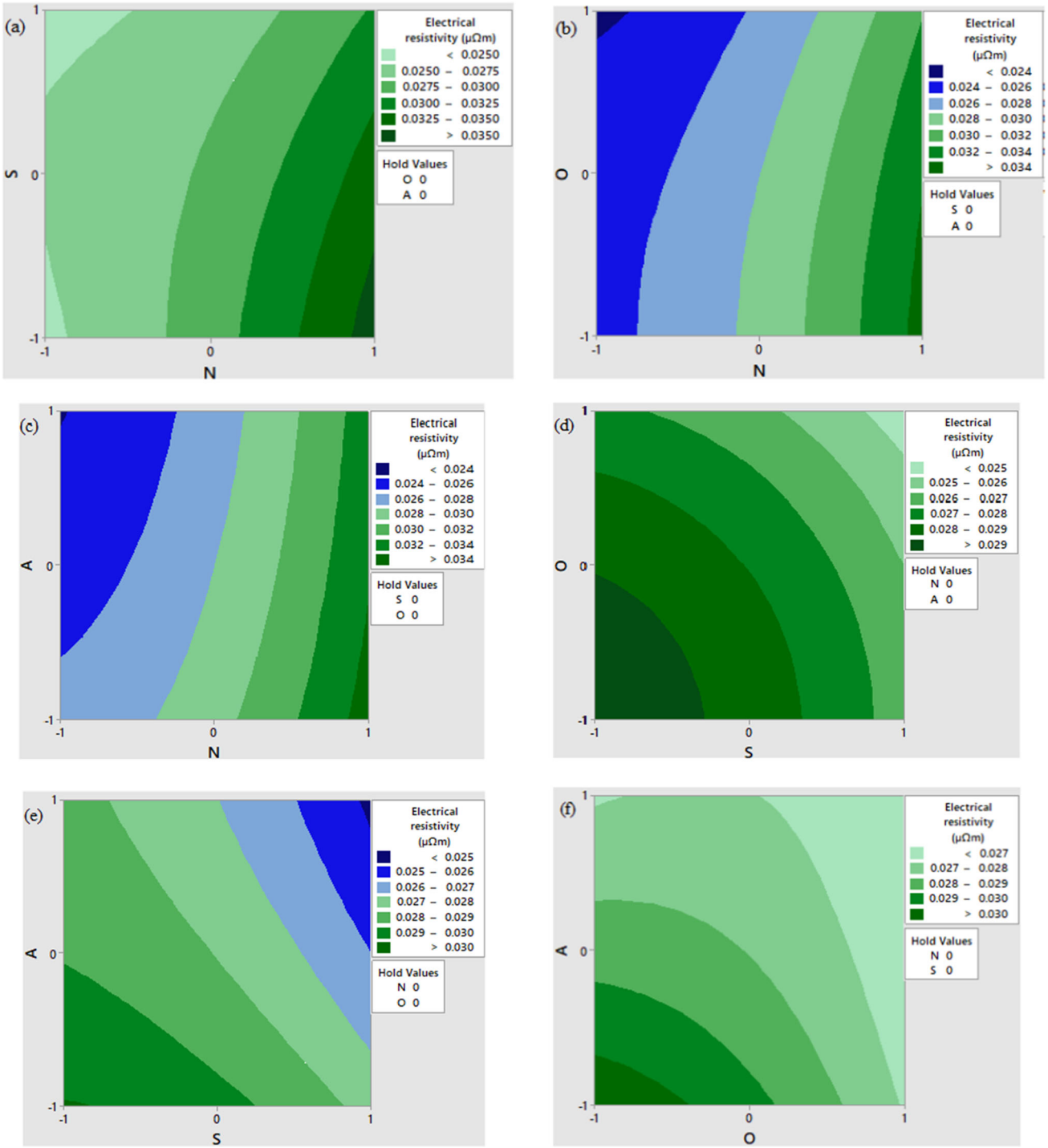

Fig. 13 Contour plots of significance of UAFSW process parameters on ρ

with greater R^2 values near 1 and also the lower standard error values specify the experimental correlation is competently realistic. It can be applied for accurate prediction of the results. The more useful variables in the generated model are specified by a higher R^2 adjusted value in the experiment. According to the statistical information in Table 4, that has a higher R^2 value of 0.979 and an adjusted R^2 value of 0.954. The statistical information shown in Table 8, however, it was revealed that for the higher R^2 value was 0.979. The corrected R^2 value was 0.956. Table 5 and Table 9 give the results of the confirmation tests results for the variables σ_s and ρ. Table

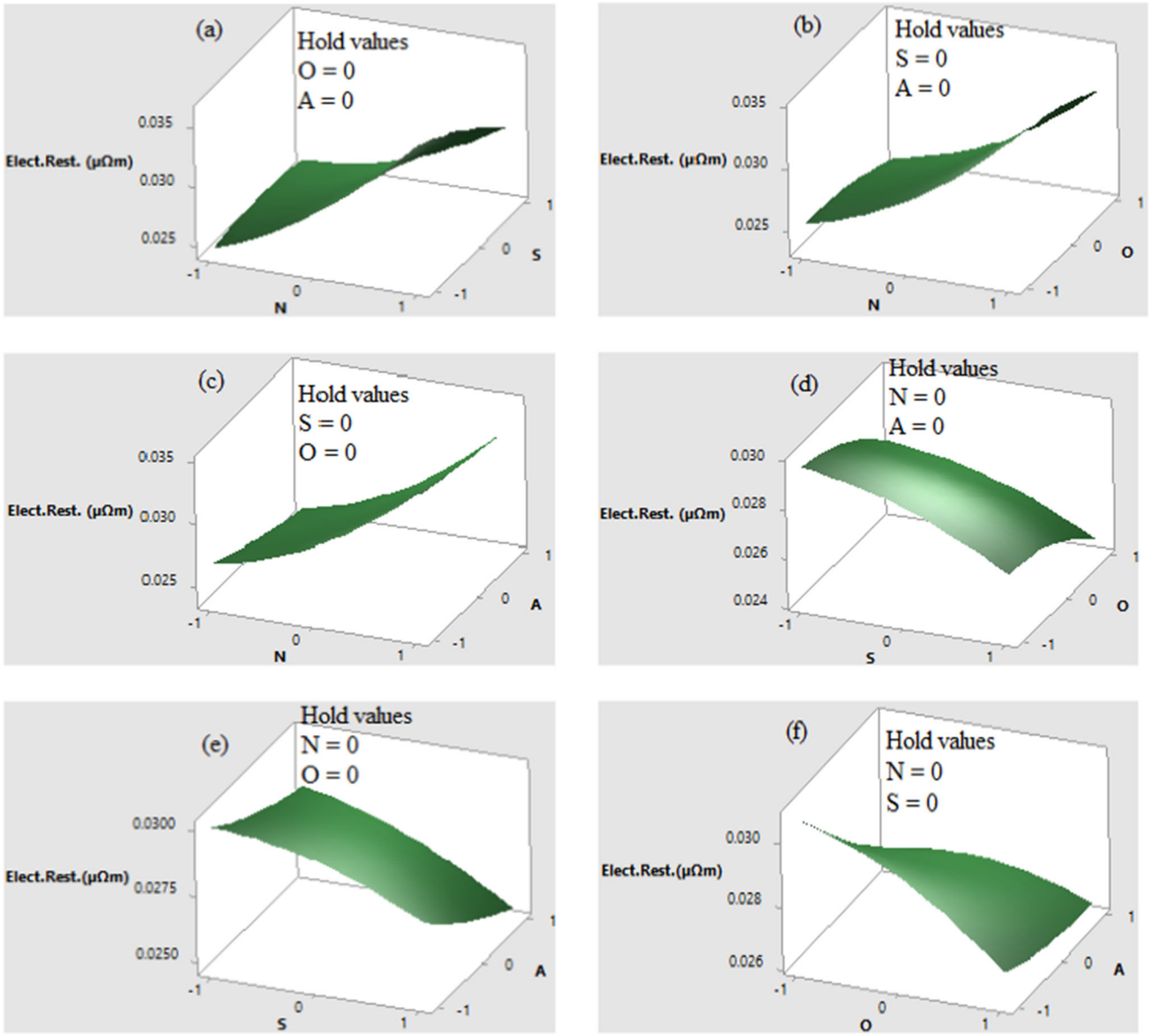

Fig. 14 Electrical resistivity plots with UAFSW parameters

6 and Table 10, respectively, presents the findings of the validation test with negligible error for the variables σ_s and ρ.

6.4 Process parameter optimization for UAFSW

The UAFSW input process parameters were optimized for the expected result in order to achieve the maximum tensile strength of the weld joint. MINITAB V17 software was used for optimization during the experimentation. In the process of optimization, the regression equation obtained from the mathematical model functions as the objective function. The optimum values were: tool rotational speed—930 rpm, traverse speed—47 mm/min, tool pin offset—1.10 mm, and tool tilt angle 2° to forecast the tensile strength of 197.66 MPa. However, the values for the most effective input UAFSW parameters for a expected electrical resistivity of 0.0227 were 708 rpm, 70 mm/min for the traverse speed, 1.20 mm for the tool pin offset, and 3° for the tool tilt angle. Tables 7 and 11 indicate the significance of the UAFSW input process parameters on tensile strength and electrical resistivity. The tool pin offset and tool rotational speed was found significant parameters in determining the tensile strength of the weld joint. For electrical resistivity of the welded joint, every process parameter was found to be significant.

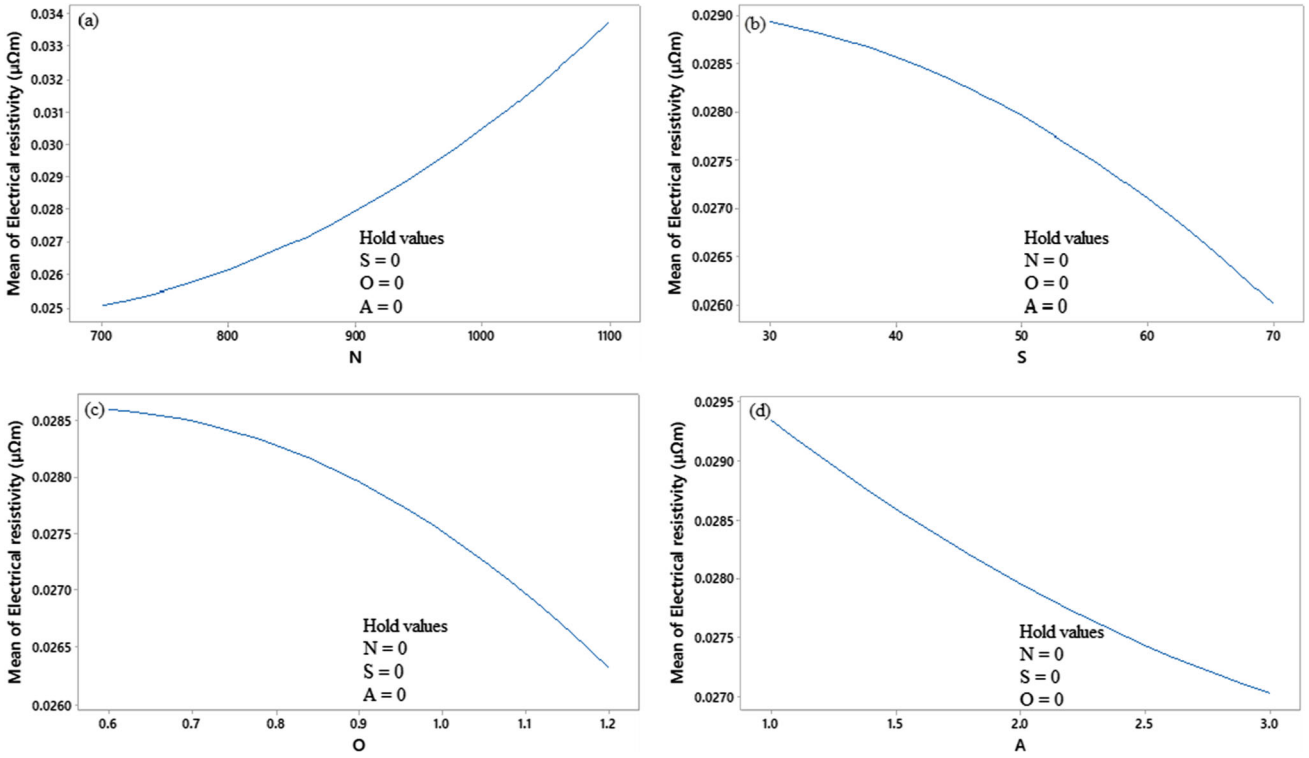

Fig. 15 Significance of UAFSW parameters on ρ include: **a** N, **b** S, **c** O, and **d** A

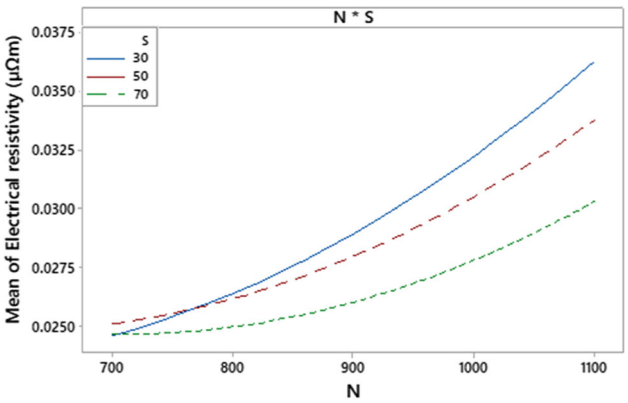

Fig. 16 Significance of N and S interacting on ρ

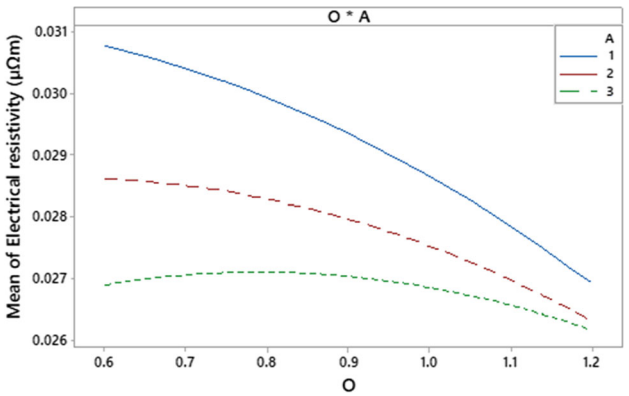

Fig. 17 Significance of N and S interacting on ρ

6.5 Weld joint microhardness test

The top zone (0.5 mm), middle zone (2 mm), and bottom zone (3.5 mm) of the weld joint were all subjected to the microhardness test across the weld direction. The tested regions exhibited variations in the microhardness distribution. The microhardness distribution is significantly influenced by ultrasonic vibrations due to softening and efficient plastic deformation [69]. The lower microhardness distribution was seen in the bottom zone. The TMAZ and HAZ region on the Cu side was found to be smaller than on the Al side. At the TMAZ, there was a smaller variation in the distribution of microhardness. Uniform microhardness distribution was observed in all the regions of the weld joint.

6.5.1 Microhardness distribution in the top region

Figure 19a shows the distribution of microhardness in the top region. The SZ showed a little complex distribution of

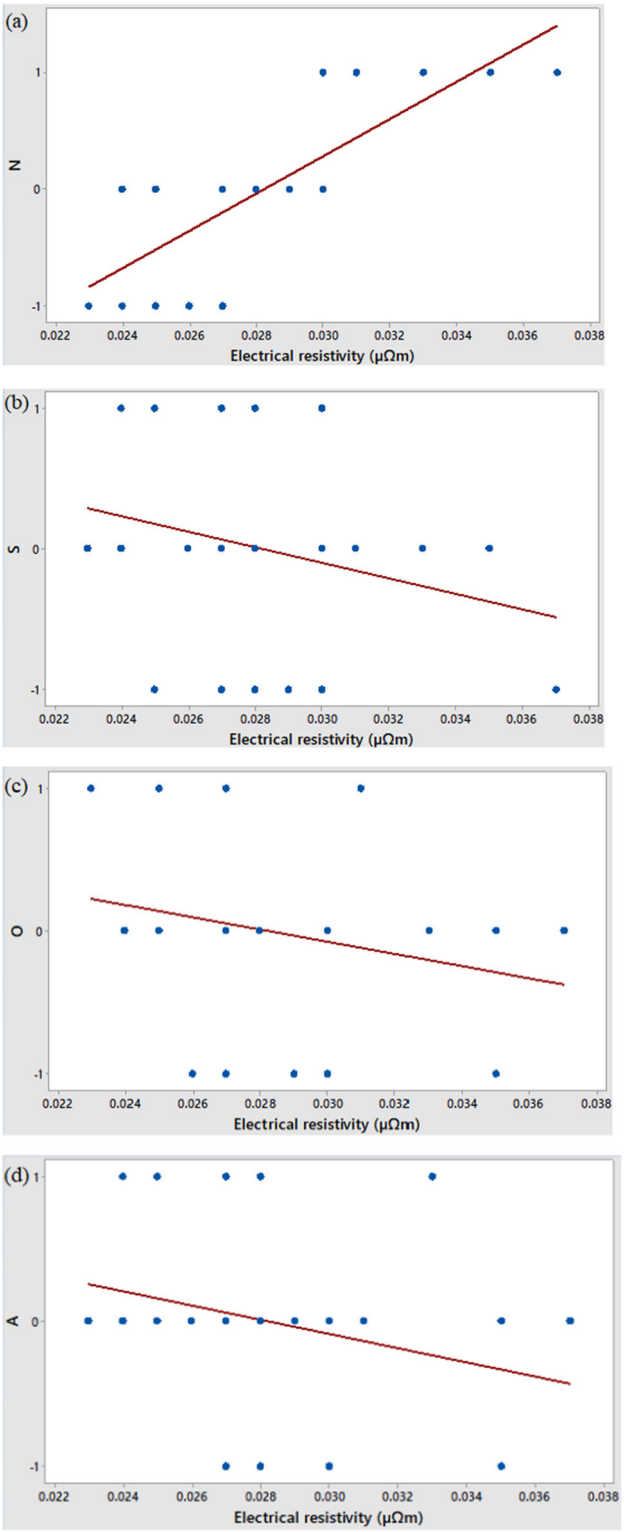

Fig. 18 Scatter plots of UAFSW input process parameters and ρ

Table 4 Statistical results for UTS

Response	R^2	Adjusted R^2	Standard error %
UTS	0.979	0.954	1.89487

microhardness upto the peak of 180 HV as ultrasonic vibrations reduces the IMCs formation and it's size. Also the lower variation in the microhardness was seen in the SZ. The microhardness distribution at the HAZ of Al side was between 40 to 50 HV. In the TMAZ of the weld joint, there was no quick peak in the distribution of microhardness was seen. The microhardness distribution at the HAZ of Cu side was of 60 HV. The ultrasonic vibrations distribute the uniform microhardness distribution [69].

6.5.2 Microhardness distribution in the middle region

Figure 19b shows the distribution of middle zone microhardness distribution. The microhardness distribution of 50 HV was seen at the HAZ of Al side of the weld joint. The peak variation upto 220 HV in the microhardness distribution was seen in the SZ. The microhardness distribution at the HAZ of Al side was of 80 HV. The TMAZ of the weld joint did not exhibit a sharp peak in the microhardness.

6.5.3 Microhardness distribution in the bottom region

In the bottom zone of the welded joint, as presented in Fig. 19c, a lower microhardness distribution is produced by the material's exciting grain refinement [69]. No peak microhardness distribution was seen. The microhardness was observed to have slightly decreased from 50 to 40 HV on the HAZ of Al side of the weld join. The peak microhardness distribution upto 190 HV was seen in the SZ. The TMAZ of the weld joint did not shown a peak in the microhardness. The microhardness distribution at the HAZ of Cu side was of 60 HV.

6.6 Fractographic analysis

The samples prepared at the optimum process parameters failed in the HAZ of the retreating side (Al side). The samples were failed in ductile manner due to the very fine recrystallized grain structure present as a result of glowing plastic deformation. Samples failed in this area serves good tensile strength [50, 52]. The fracture location and fractured sample images of the tensile test samples are shown in Table 12.

Table 5 UAFSW validation experiment results for UTS

Experimental run no	Input process parameter				σ_s (MPa)		Error σ_s %
	N	S	O	A	Experimental value	Predicted value	
1	1100	70	0.9	2	180.10	181.3876	0.7098
2	700	30	0.9	2	171.50	172.9021	0.8101
3	900	50	0.6	3	190.36	191.0578	0.3652
4	1100	30	0.9	2	179.20	181.6821	1.3661
5	700	70	0.9	2	170.70	171.3876	0.4011

Percentage error = [(Experimental value – Predicted value)/Predicted value] × 100% [58]

Table 6 Tensile strength confirmation test results

Experimental run no	Input process parameters				σ_s (MPa)		Error σ_s %
	N	S	O	A	Experimental value	Predicted value	
1	930	47	1.10	2	197.15	197.6633	0.2596

Table 7 ANOVA results for tensile strength

Source	DF	Adj SS	Adj MS	F-Value	*P* Value	Significance of process parameter [68]
Model	14	2007.94	143.42	39.95	0.000	–
Linear	4	298.55	74.64	20.79	0.000	–
N	1	264.52	264.52	73.67	0.000	Yes
S	1	2.32	2.32	0.64	0.438	No
O	1	30.47	30.47	8.49	0.013	Yes
A	1	0.62	0.62	0.17	0.684	No

Table 8 The electrical resistivity statistics

Response	R^2	Adjusted R^2	Standard error %
Electrical resistivity	0.979%	0.956%	0.0007380

6.7 Discussion

In this research work the enhanced tensile and electrical properties were observed with the application of ultrasonic vibrations with traditional FSW process. This research work suggests the set of optimum values of the input process parameters of UAFSW process for achieving maximum tensile strength and minimum electrical resistivity of the weld joint. So, this research optimization helps to reduce the trial and error of the UAFSW process and obviously reduces the cost of the process with enhanced mechanical and electrical properties.

Table 9 Results of electrical resistivity test validation

Experimental run no	Input process parameters				ρ (μΩm)		Error %
	N	S	O	A	Experimental value	Predicted value	
1	900	70	1.2	3	0.025	0.0240	4.16
2	900	30	0.9	1	0.030	0.0301	0.33
3	900	50	0.6	3	0.027	0.0269	0.37
4	900	70	0.9	1	0.028	0.0277	1.08
5	1100	50	1.2	2	0.032	0.0319	0.31

Percentage error = [(Experimental value–Predicted value)/Predicted value] × 100% [58]

Table 10 Electrical resistivity confirmation test results

Experimental run no	Input parameters				ρ (μΩm)		Error ρ (μΩm) %
	N	S	O	A	Experimental value	Predicted value	
1	708	70	1.20	3	0.023	0.0227	1.32%

Table 11 An ANOVA results for electrical resistivity of the weld joint

Source	DF	Adj SS	Adj MS	F-Value	*P* Value	Significance of process parameter [68]
Model	14	0.000319	0.000023	41.79	0.000	–
Linear	4	0.000283	0.000071	129.92	0.000	–
N	1	0.000225	0.000225	413.77	0.000	Yes
S	1	0.000024	0.000024	44.64	0.000	Yes
O	1	0.000015	0.000015	28.33	0.000	Yes
A	1	0.000015	0.000015	27.86	0.000	Yes

7 Conclusions

(1) The optimum input process parameters were as: tool rotational speed—930 rpm, traverse speed- 47 mm/min, tool pin offset—1.10 mm, and tool tilt angle—2° resulted in weld joints with a tensile strength of 197.15 MPa.
(2) The traverse speed and tool tilt angle were found non-significant parameters for the tensile strength of the weld joint, but the tool rotational speed and tool pin offset were significant parameters.
(3) Electrical resistivity of the welded joints was 0.023 μΩm at the optimum process parameters of: tool rotation speed—708 rpm, traverse speed—70 mm/min, tool pin offset—1.20 mm, and tool tilt angle-3°.
(4) All the input process parameters were found significant for electrical resistivity of the weld joint.
(5) The peak microhardness distribution across the weld direction was seen as: top zone > middle zone > bottom zone.
(6) The samples of optimum tensile strength test failed in HAZ of the weld joint.

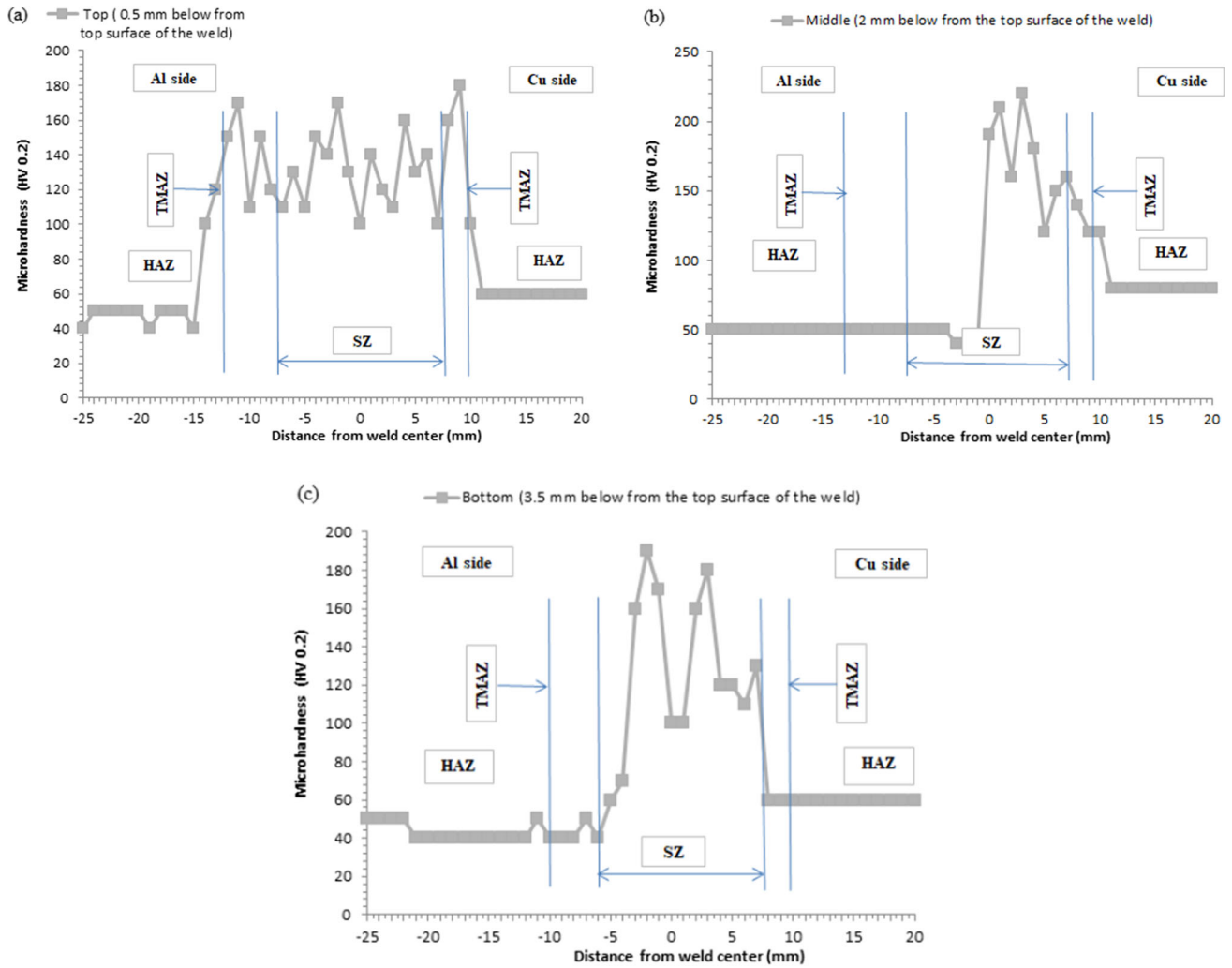

Fig. 19 Microhardness distribution at a set of UAFSW optimized process parameters as: N = 930 rpm, S = 47 mm/min, O = 1.10 mm, A = 2°

Table 12 Fracture location of the weld joints prepared for validation test

Experimental run no	Fracture location	Image of fractured sample
1	TMAZ (advancing side)	
2	SZ	
3	HAZ (retreating side)	
4	TMAZ (advancing side)	
5	TMAZ (advancing side)	

References

1. Park K., Kim G., and Ni J.: Design and analysis of ultrasonic assietd friction stir welding. in ASME, International Mechanical Engineeering Congress & Exposition, Proceedigs of IMECE, pp. 1–7, (2007).
2. Tian, W., Su, H., Wu, C.: Effect of ultrasonic vibration on thermal and material flow behavior, microstructure and mechanical properties of friction stir welded Al/Cu joints. Int. J. Adv. Manufact. Technol. **104**, 1–13 (2020)
3. Ahamadina, M., Seidanloo, A., Rostamiyan, Y., Teimouri, R.: Determining influence of ultrasonic-assisted friction stir welding parameters on mechanical and tribological properties of AA6061 joints. Int. J. Adv. Manufact. Technol. **78**, 1–16 (2015)
4. Section IV, Chapter 13, "Bus conductor design and applications", 1–70.
5. Shojaeefard, M., Khalkhali, A., Bhattacharya, O., Tahani, M.: Application of Taguchi optimization in determining aluminum to brass friction stir welding parameters. Mater. Des. **52**, 587–592 (2013)
6. Kerrar, G., Merah, N., Shuaib, A., Badour, F., Bazoune, A.: Experimental and numerical investigations on friction stir welding of aluminum to copper. Appl. Mech. Behav. Mater. Eng. Syst. **2017**, 129–138 (2017)
7. Esmaeili, A., Besharathi, M.K., Zareie Rajani, H.R.: Experimental investigation of material flow and welding defects in friction stir welding of aluminum to brass. Mater. Manufact. Processes **27**, 1402–1408 (2012)
8. Felix, M., Jayabalan, V.: Tool traverse speed effects on the microstructure of friction stir welded aluminum-copper joint. J. Mater. Process. Technol. **217**, 105–113 (2015)
9. Li, X.-W., Zhang, D.-T., Qiu, C., Zhang, W.: Microstructure and mechanical properties of dissimilar pure copper/1350 aluminum alloy butt joints by friction stir welding. Trans. Nonferrous Metals **22**, 1298–1306 (2012)
10. Gao, S., Wu, C., Padhy, G.: Effect of leding ultrasonic vibrations on the welding forces of friction stir lap welding. Int. J. Adv. Manufact. Technol. **104**, 3181–3189 (2019)
11. Hong, K., Wang, Y., Zhou, J., Zhou, C., Wang, L.: Investigation on ultrasonic assisted friction stir welding of aluminum/steel dissimilar alloys. High Temperature Mater. Processses **40**, 45–52 (2021)
12. Liu, H., Shen, J., Zhou, L., Kuang, L.: Microstructural characterization and mechanical properties of friction stir welded joints of aluminum alloy to copper. Sci. Technol. Weld. Joining **16**, 92–98 (2011)
13. Fotouchi, Y., Rasaee, S., Askari, A., Bisadi, H.: Effect of traverse speed of the tool on microstructure and mechanical properties in dissimilar butt friction stir welding of Al5083-copper sheets. Eng. Solid Mech. **2**, 239–246 (2014)
14. Dharmalingam, S., Lenin, K.J.: Effect of friction stir welding parameters on microstructure and mechanical properties of the dissimilar AA7475-AA8011 joints. Mater. Today **39**, 1–5 (2020)
15. Delrue, A., Tabatabaeipour, M., Hettler, J., Abeele, K.: Alllying a nonlinear, pitch-catch, ultrasonic technique for the detection of kissing bonds in friction stir welds. Ultrasonics **68**, 71–79 (2016)
16. Shi, L., Wu, C., Gao, S.: Analysis of welding load reduction in ultrasonic vibration-enhanced friction stir welding. Int. J. Adv. Manufact. Technol. **99**, 373–385 (2018)
17. Singh, R., Khamba, J.: Ultrasonic machining of Titanium and its alloys: a review. J. Mater. Process. Technol. **173**, 125–135 (2006)
18. Baradarani, F., Mostafapour, A., Shalvandi, M.: Effect of ultrasonic assisted friction stir welding on microstructure and mechanical propertis of AZ91-C magnesium alloy. Trans. Nonferrous Met. Soc. China **29**, 2514–2522 (2019)
19. Hu, Y., Liu, H., Fujii, H.: Improving the mechancal properties of 2219–T6 aluminum alloy jointsby ultrasonic vibrations during friction stir welding. J. Mater. Process. Tech. **271**, 75–84 (2019)
20. Baradarani, F., Mostafapour, A., Shalavandi, M.: " Enhanced corrosion behavior and mechanical properties of AZ91 magnesium alloy developed by ultrasonic-assisted friction stir welding. Mater. Corrosion **17**, 1–7 (2019)
21. Kumar, S., Wu, C.: A novel techniue to join Al and Mg alloys: ultrasonic vibration assisted linear friction stir welding. Mater. Today Proc. **5**, 18142–18151 (2018)
22. Shahreza, A., Amini, S.: Experimental comparison of the effects of superimposed axial and bending ultrasonic vibrations on friction stir welding process. J. Eng. Manufact. **233**, 539–552 (2017)
23. Kumar, S.: Ultrasonic assisted friction stir processing of 6063 aluminum alloy. Arch. Civil Mech. Eng. **16**, 473–484 (2016)
24. Ma, H., He, D., Liu, J.: Ultrasonically assisted friction stir welding of aluminum alloy 6061. Sci. Technol. Weld. Joining **20**, 216–221 (2014)
25. Amini, S., Amiri, M.: Study of vibration's effect on friction stir welding. Int. J. Adv. Manuf. Technol. **73**, 127–135 (2014)
26. Thoma, M., Wagner, G., Stra, B., Conrad, C., Wolter, B., Benfer, S., Furbeth, W.: Recent developments for ultrasonic-assisted friction stir welding: joining, testing, corrosion- an overview. Mater. Sci. Eng. **118**, 1–7 (2016)
27. Zhang, Z., He, C., Li, Y., Zhao, S., Zhao, X.: Effects of ultrasonic assisted friction stir welding on flow behavior, microstructure and mechanical properties of 7N01-T4 aluminum alloy joints. J. Mater. Sci. Technol. **43**, 1–13 (2020)
28. Alexander, E., Sergei, T., Sergei, F., Valery, R., Tatiana, K.: Effect of ultrasonic application during friction stir welding on microstructure and properties of AA2024 fixed joints. Key Eng. Mater. **683**, 227231 (2016)
29. Liu, Y., Lu, S.: Effects of ultrasonic vibrations on the welding process of friction stir welding. Mater. Sci. Forum **850**, 710–715 (2016)
30. Wang, T., Gong, X., Ji, S., Xue, G., LV, Z.: Ultrasonic assisted active-passive filling friction stir repairing to eliminate volume defects. Arch. Matall. Mater. **66**, 217–222 (2021)
31. Oanca, O., Mnerie, G., Binchiciu, E., Cojocaru, R., Botila, L., Duma, I.: Research on the welding behavior for alloy EN AW 5754 when using FSW-US hybrid process. Adv. Mater. Res. **1153**, 92–97 (2019)
32. Singh, P.: Investigation on the effect of mechanical vibration in mild steel weld pool. Manufacturing Rev. **6**, 1–11 (2019)
33. Ruilin, L., Diqia, H., Lucheng, L., Shaoyong, Y.: A study of the temperature field during ultrasonic-assisted friction stir welding. Int. J. Adv. Manufact. Technol. **73**, 321–327 (2014)
34. Ohrdes, H., Nothdurft, S., Nowroth, C., Grajczak, J., Twiefel, J., Hermsdof, J., Kaierle, S., Wallaschek, J.: Influence of the ultrasonic vibration amplitude on the melt pool dynamics and the weld shape of laser beam welded EN AW-6082 utilizing a new excitation system for laser beam welding. Product. Eng. **15**, 151–160 (2021)
35. Bagheri, B., Abbasi, M., Abdollahzadeh, A.: Microstructure and mechanical characteristics of AA6061-T6 joints produced by friction stir welding, friction stir vibration welding and Tunsten inert gas welding: a comparative study. Int. J. Minerals, Metall. Mater. **28**, 450–460 (2021)
36. Xue, F., He, D., Haibo, Z.: Effect of ultrasonic vibration in friction stir welding of 2219 aluminum alloy: an effective model for predicting weld strength. Metals **12**, 1–17 (2022)
37. Tarasov, S., Rubtsov, V., Fortuna, S., Eliseev, A., Chumaevsky, A., Kalashnikova, T., Kolubaev, E.: Ultrasonic-assisted aging in friction stir welding on Al-Cu-Li-Mg aluminum alloy. Weld world **61**, 1–10 (2017)

38. Thoma, M., Gester, A., Wanger, G., Stra, B., Wolter, B., Benfer, S., Gowda, D., Furbeth, W.: Application of the hybrid process ultrasound enhanced friction stir welding on dissimilar aluminum/dual phase steel and aluminum/magnesium joints. Materialwiss **50**, 893–912 (2019)
39. Wazery, M., Mabrouk, O., Elsissy, A.: Optimization of ultrasonic-assisted friction stir welded using Taguchi appproach. IJE Transactions **35**, 213–219 (2022)
40. Mehdi, H., Batra, L., Singh, A.P.: Multi-response optimization of FSW process parameters of dissimilar aluminum lloys of AA 2014 and AA 6061by response surface methodology. Int. J. Interactive Design Manufact. **27**, 1–6 (2023)
41. Mehdi, H., Mehmood, A., Chinchkar, A., Hashmi, A., Malla, C., Mohapatra, P.: Optimization of process parameters on the mechanical properties of AA6061/Al_2O_3 nanocomposites fabricated by multi-pass friction stir processing. Mater. Today: Proceed. **56**(4), 1995–2003 (2022)
42. Salah, A., Mehdi, H., Mehmood, A., Hashmi, A., Malla, C., Kumar, R.: Optimization of process parameters for friction stir welded joints of dissimilar aluminum alloys AA3003 and AA 6061 by RSM. Mater. Today **56**(4), 1675–1683 (2022)
43. Bhatnagar, S., Kumar, G., Mehdi, H., Kumar, M.: Optimization of FSW parameters for enhancing dissimilar joint strength of AA 7075 and AA 6061 using Response Surface Methodology (RSM). Mater. Today **19**, 1–13 (2023)
44. Galvao, I., Loureiro, A., Verendra, D., Gesto, D., Rodrigues, D.: Influence of tool offsetting on the structure and morphology of dissimilar aluminum to copper friction stir welds. Metall. Mater. Trans. **43A**, 5096–5105 (2012)
45. Celik, S., Cakir, R.: Effect of friction stir welding parameters on the mechanical and microstructure properties of the Al-Cu butt joint. Metals **6**, 1–15 (2016)
46. Al-Roubaiy, A.O., Nabat, S., Batako, A.: Experimental and theoretical analysis of friction stir welding of Al-Cu joints. Int. J. Adv. Manufact. Technol. **71**, 1631–1642 (2014)
47. Beygi, R., Kazeminezhand, M., Kokabi, A.H.: Butt joining of Al-Cu bilayer sheet through friction stir welding. Trans. Nonferrous Metals **22**, 2925–2929 (2012)
48. Akinlabi, E., Akinlabi, S.: Effect of heat input on the properties of dissimilar friction stir welds of aluminum and copper. Amer. J. Mater. Sci. **2**, 147–152 (2012)
49. Mehta, K.P., Badheka, V.J.: Influence of tool pin design on properties of dissimilar copper to aluminum friction stir welding. Trans. Nonferrous Metals **27**, 36–54 (2017)
50. Xue, P., Ni, D.R., Wang, D., Xiao, B.L., Ma, Z.Y.: Effect of friction stir welding parameters on the microstructure and mechanical properties of the dissiimilar Al-Cu joints. Mater. Sci. Eng. **528**, 4683–4689 (2011)
51. Mehdi, H., Mishra, R.S.: Effect of friction stir processing on mechanical properties and heat transfer of TIG welded joint of AA6061 and AA 7075. Defecnce Technol. **17**, 715–727 (2021)
52. Barekatain, H., Kazeminezhad, M., Kokabi, A.H.: Microstructure and mechanical properties in dissimilar butt friction stir welding of severely plastic deformed aluminum AA1050 and commercially pure copper sheets. J. Mater. Sci. Technol. **30**, 1–9 (2013)
53. Wang, X., Yuan, X., Ning, J., Li, X.: Influence of interfacial intermetallic compounds on electrical characterization of Cu/Al joints produced by flash welding and diffusion brazing. Mater. Res. **23**, 1–10 (2020)
54. Nirgude S. and Kalpande S.: Parametric optimization of friction stir welding of AA 6101 T-64 and pure Cu using response surface methodology", International Journal on Interactive Design and Manufacturing (IJIDeM), pp. 1–19, (2023).
55. Kakade, S.P., Thakur, A.G., Deshmukh, D.D., Patil, S.B.: Experimental investigations and optimisation of Ni-Cr-B-Si hardfacing characteristics deposited by PTAW process on SS 410 using response surface method. Adv. Mater. Process. Technol. **13**, 1–17 (2022)
56. Deshmukh, D.D., Kharche, Y.: Influence of processing conditions on the tensile strength and failure pattern of resistance spot welded SS 316L sheet joint. Int. J. Interactive Design Manufact. **2023**, 1–13 (2023)
57. Deshmukh, D.D., Kalyankar, V.D.: Analysis of deposition efficiency and distortion during multitrack overlay by plasma transferred arc welding of Co-Cr alloy on 316L stainless steel. J. Adv. Manuf. Syst. **20**(4), 705–728 (2021)
58. Shanavas, S., Dhas, J.E.: Parametric opimization of friction stir welding parametrs of marine grade aluminum alloy using response surface methodology. Trans. Nonferrous Metals Soci. China. **27**, 2334–2344 (2017)
59. Zhang, J., Shen, Y., Yao, X., Xu, H., Li, B.: Investigation on dissimilar underwater friction stir lap welding of 6061 T-6 aluminum alloy to pure copper. Mater. Des. **64**, 74–80 (2014)
60. Muhammad, N., Wu, C., Padhy, G.K.: Review: progress and trends in ultrasonic assisted friction stir welding. J. Harbian Inst. Technol. **25**(3), 16–42 (2018)
61. Padhy, G.K., Wu, C.S., Gao, S., Shi, L.: Local microstructure evolution in Al 6061–T6 friction stir weld nugget enhanced by ultrasonic vibration. Mater. Des. **92**, 710–723 (2016)
62. Liu, X., Wu, C., Padhy, G.: Improved weld macrosection, microstructure and mechanical properties of 2024 Al T-4 butt joints in ultrasonic vibration enhanced friction stir welding. Sci. Technol. Weld. Joining **20**, 345–352 (2015)
63. Bisadi, H., Tour, M., Tour, S.: The influences of rotational and welding speeds on microstructures and mechanical properties of friction stir welded Al5083 and commercially pure copper sheets lap joints. Mater. Des. **43**, 80–88 (2013)
64. Manickam, S., Balsubramanian, V.: Optimizing the friction stir spot welding parameters to attain maximum strength in Al-Mg dissimilar material joining. J. Weld. Joining **34**, 23–31 (2016)
65. Mehdi H., Jain S., Mabuwa S., and Malla C., " Effect of intermetallic compounds on mechanical and microstructural properties of dissiilar alloysAl-7Si/AZ91D", Journal of Materials Engineering and Performance, (2023).
66. Khajeh, R., Jafarian, H., Seyedein, S., Jabraeili, R., Eivani, A., Park, N., Kim, Y., Heidarzadeh, A.: Microstructure, mechanical and electrical properties of dissimilar friction stir welded 2024 aluminum alloy and copper joints. J. Mater. Res. Technol. **14**, 1945–1957 (2021)
67. Singh, Y.: Electrical resistivity measurements: a review. Int. J. Modern Phys. **22**, 745–756 (2013)
68. Deshmukh, D.D., Kalyankar, V.D.: Deposition characteristics of multitrack overlay by plasma transferred arc welding on SS316 with Co-Cr based alloy-influence of process parameters. High Temperat. Mater. Processes **46**, 248–263 (2018)
69. Gao, S., Wu, C., Padhy, G.: Material flow, microstructure and mechanical properties of friction stir welded AA 2024–T3 enhanced by ultrasonic vibrations. J. Manuf. Process. **30**, 385–395 (2017)